Local domain inversion in MgO-doped lithium niobate by pyroelectric field-assisted femtosecond laser lithography

Jörg Imbrock, Haissam Hanafi, Mousa Ayoub, and Cornelia Denz

Citation: Appl. Phys. Lett. **113**, 252901 (2018); doi: 10.1063/1.5053870
View online: https://doi.org/10.1063/1.5053870
View Table of Contents: http://aip.scitation.org/toc/apl/113/25
Published by the American Institute of Physics

Local domain inversion in MgO-doped lithium niobate by pyroelectric field-assisted femtosecond laser lithography

Jörg Imbrock,[a)] Haissam Hanafi, Mousa Ayoub, and Cornelia Denz
Institute of Applied Physics and Center for Nonlinear Science, University of Münster, Corrensstr. 2, 48149 Münster, Germany

(Received 27 August 2018; accepted 1 December 2018; published online 18 December 2018)

We explore a physical approach to invert ferroelectric domains in the volume of MgO-doped lithium niobate crystals without any external electric field. Permanent defect structures are created by focused infrared femtosecond laser pulses below the material surface along the polar axis followed by a thermal treatment. This procedure leads to an inversion of ferroelectric domains beneath and above the laser-induced filaments up to the surfaces of the crystal. All domain walls are straight and up to 800 μm long. We measure the domain width in dependence on the length of the filaments and the writing energy. The smallest achieved domain width and the domain spacing is 1 μm. We propose a model taking into account the temperature dependence of the pyroelectric field and thermally activated bulk charges to explain the mechanism of domain inversion. Our findings pave the way to all-optical printing of arbitrary ferroelectric domain structures for nonlinear photonic applications. *Published by AIP Publishing.* https://doi.org/10.1063/1.5053870

Ferroelectric domain engineering comprises the creation of tailored stable domains in ferroelectric crystals. Crystals with domain engineered structures like widely used periodically poled lithium niobate (PPLN) play an important role in nonlinear optics for quasi-phase-matched parametric processes such as second-harmonic generation (SHG) and difference frequency generation.[1–3] An established technique for ferroelectric domain inversion is the application of an electric field larger than the coercive field along the direction of spontaneous polarization via patterned electrodes.[4] PPLN crystals are commercially available with poling periods down to a few micrometers. While electrical poling is conventionally applied,[5] there is also strong interest in more flexible fabrication methods that use light to modulate the nonlinearity. Optical structuring allows for high resolution, and moreover, some light-mediated domain inversion processes do not require an external electric field at all.

The highest conversion efficiencies are generally realized in a quasi-phase-matched parametric process, where the nonlinear polarization is switched by 180°, i.e., when ferroelectric domains are inverted. However, it is not entirely necessary to alternate the sign of the nonlinearity between $+\chi^{(2)}$ and $-\chi^{(2)}$, because modulation of the nonlinearity is already sufficient to achieve quasi-phase matching. It was shown that focused fs-laser pulses can locally decrease the nonlinearity in lithium niobate ($LiNbO_3$), thus creating a weakly modulated quasi-phase matching structure.[6] We have used this technique recently to fabricate integrated quasi-phase matched waveguides in $LiNbO_3$.[7] The advantage of this method is that the nonlinearity can be modulated in three dimensions (3D).[8] However, due to the weak modulation of the nonlinearity, the conversion efficiency is smaller compared with electrically inverted ferroelectric domain structures.

Light-based ferroelectric domain inversion can be classified into two categories:[9] *light-assisted poling* and *all-optical poling*. Light-assisted poling typically involves an ultraviolet (UV) laser to assist classical electrical poling. In this scheme, an external field is applied during a structured continuous wave (cw) illumination.[10,11] Because of the high absorption of UV light, this illumination leads to a modulation of the coercive field which in turn results in a domain inversion.[12,13] All-optical poling as the second light-based method can be achieved with cw or pulsed laser light. Here, the local inversion of domains is based on an induced pyroelectric or thermoelectric field.[14–20] However, the domain length is restricted in both cases to a few hundred nanometers due to the strong absorption in this wavelength regime.

Recently, a promising all-optical domain inversion process was demonstrated with focused fs-laser pulses in $LiNbO_3$.[21–23] $LiNbO_3$ is transparent in this wavelength range, i.e., linear absorption can be neglected. The focused infrared (IR) pulses cause local heating by multiple photon absorption, leading to a local reduction of the coercive field and to an internal field that exceeds the threshold field of domain nucleation. This in turn leads to domain inversion at the position of the laser focus. These domains have a conical shape, and the maximum reported domain length is about 60 μm, which is shorter than the thickness of the crystal used.[21] The domain length is limited in this process because the laser focus is elongated in the depth of the crystal due to spherical aberrations induced by the high refractive index n of $LiNbO_3$, and it also splits into multiple foci because of birefringence.[24,25]

Here, we present a domain inversion approach in MgO-doped $LiNbO_3$ that is different from the methods mentioned above. It is based on a versatile combination of fs-laser lithography and global thermal treatment. By exploiting this technique which does not require any external applied electric field, we are able to create arbitrary 2D nonlinear photonic structures, while the ferroelectric domains have a high aspect ratio of domain length to domain width. We propose a model that involves thermally activated bulk charges which drift in the pyroelectric field, leading to a local space charge

---

[a)] imbrock@uni-muenster.de

field. During cooling down, the domain formation is driven by this space charge field that locally exceeds the threshold field of domain nucleation.

The experimental scheme of ferroelectric domain inversion by pyroelectric field-assisted fs-laser lithography is depicted in Fig. 1. We use *z*-cut $LiNbO_3$ crystals doped with 5 mol. % magnesium oxide (Gooch and Housego). The samples are either 0.5 mm or 1 mm thick, and the length along the *x*- and *y*-axes is 10 mm, respectively. The *z*-surfaces are polished to optical quality. The sample is mounted on a 3D translation stage in a fs-laser lithography system.[26] First, we focus fs-laser pulses by a microscope objective with a numerical aperture (NA) of 0.8 along the polar *z*-axis into a depth *z*. Then, we pull the focus out of the crystal to the surface with a velocity of 80 μm/s. Thus, the distance that the focus is moved inside the crystal is $z \cdot n$. The laser pulses have a wavelength of 800 nm, a pulse width of 100 fs, a repetition rate of 1 kHz, and energies between 50 nJ and 550 nJ. The power density at 100 nJ is 2×10^{18} W/m^2. This induction step is repeated at different positions in the *xy*-plane with the aim of writing 2D structures of permanent filaments into the $LiNbO_3$ crystal.[27–31] Afterwards, the sample is heated in an oven to 200 °C and then cooled down to room temperature. The heating and cooling rates are approximately 5 °C/min.

The domain structures that are built after cooling down are visualized at the crystal surfaces by selective chemical etching in HF acid (48% HF and 65% HNO_3) for 2 h. The different etch rates along the $+z$- and $-z$-axes lead to a surface profile that is imaged with a bright field microscope. The domain boundaries are also imaged in the volume of the crystals by Čerenkov laser scanning SHG microscopy.[32] A detailed description of our Čerenkov SHG microscope can be found elsewhere.[33] The operational principle is as follows: a tightly focused laser pulse (800 nm, 80 fs, 80 MHz, NA = 0.79) is scanned in the *xy*-plane in different depths in the crystal. Whenever the laser focus passes a domain wall, Čerenkov SHG is generated. The second harmonic is imaged by a condenser lens, and its intensity is measured with a photomultiplier. The lateral resolution is approximately 1 μm. Čerenkov SHG microscopy is also able to detect structural modifications in the crystal volume written by focused fs-laser pulses.[8,25] The difference is that only domain boundaries give rise to Čerenkov SHG and not the inner part,[32,33] whereas a laser-induced filament is completely visible in SHG microscopy.[8,25]

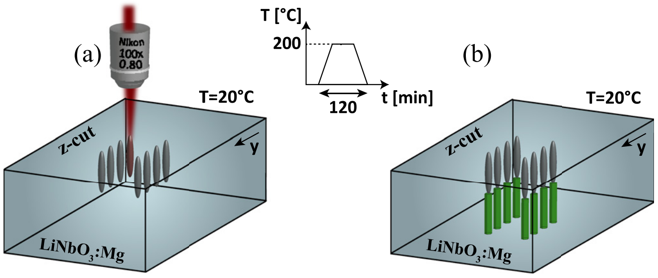

FIG. 1. Experimental scheme. (a) Fs-laser pulses are focused with a microscope objective (NA = 0.8) along the *z*-axis and pulled out of the sample to induce permanent filaments (grey). The sample is heated up to 200 °C and then cooled down. (b) Ferroelectric domains (green) are inverted below the filaments after cooling down.

We have systematically investigated filaments created below the crystal surface with respect to different pulse energies and also changed the investigated length of the filaments (Fig. 2). The energy was increased from 200 nJ to 550 nJ (from left to right), and the pulses were initially focused to a depth of 100 μm and then pulled to the surface. All filaments have a width of about 2 μm, and the length slightly increases with increasing pulse energy [Fig. 2(a)]. After this induction process, no ferroelectric domains are inverted yet. The filaments themselves appear dark in a bright field microscope, and they are permanent, i.e., their shape remains after the thermal treatment. After the thermal treatment, however, domains have been formed below the filaments [Fig. 2(b)]. Ferroelectric domains are inverted below the filaments after cooling down, independent of the propagation direction of the laser pulses with respect to the *z*-axis during the induction process. There was no substantial difference in the results if the pulse entered the crystal from the $-z$- or $+z$-surface or if the laser pulse was pushed into the crystal instead of pulled towards the surface. The longest domain that we could produce with this technique in a 1 mm thick sample formed below a 200 μm long filament was 800 μm long [Fig. 2(c)]. Figure 3 shows a Čerenkov SHG microscopy image of ferroelectric domains in the *xy*-plane at the bottom of the crystal. Each filament above the domains was induced with a different pulse energy (rows) and at a different depth (columns). The typical hexagonal domain shape becomes clearly visible. The domains that reach the bottom of the crystal exhibit straight domain boundaries as can be seen in the 3D image of the single domain in Fig. 3(b). This third row is shown in Fig. 2(b). The domain inversion critically depends on the pulse energy and on the length of the laser-induced filaments. We have measured the width of the domains in dependence on the pulse energy for the filaments that were addressed at a depth of 120 μm (upper row in Fig. 3). Figure 4(a) shows that no domains form after cooling down below an energy threshold, whereas above the threshold, the width of the

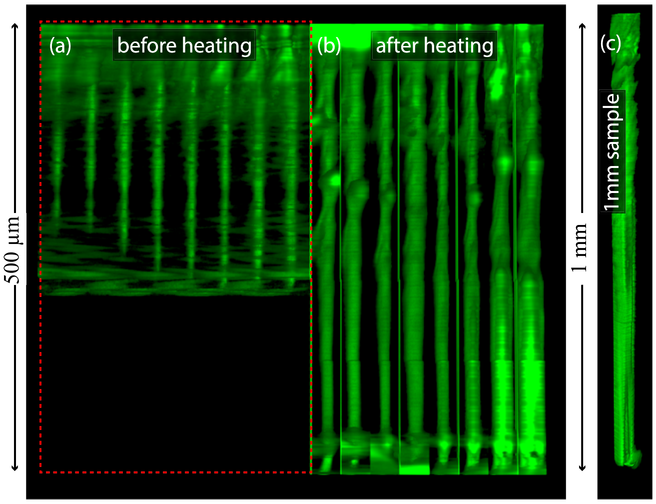

FIG. 2. SHG microscopy image of laser-induced filaments and ferroelectric domains. (a) Laser-induced filaments in the *xz*-plane before thermal treatment. The energy was increased from 200 nJ to 550 nJ and the pulses were initially focused to a depth of 100 μm and then pulled to the surface. (b) Ferroelectric domains form below filaments after thermal treatment. (c) Fabricated domain in a 1 mm thick crystal.

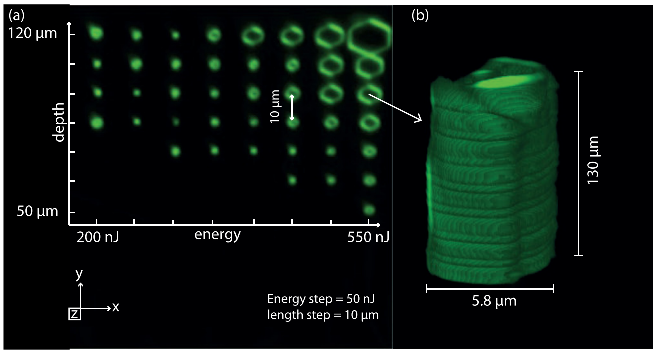

FIG. 3. (a) Čerenkov SHG microscopy image of ferroelectric domains in the *xy*-plane at the bottom of the crystal for different pulse energies and addressed depths of the laser-induced filaments. The green lines are the domain boundaries. (b) The single domain marked with an arrow is shown in detail in 3D.

domains increases with increasing pulse energy. Note that the domains located at the edge of the processed area are slightly broader compared to the domains inside the array [Fig. 3(a)]. This can be seen at the first few non-zero data values and also at the last value in Fig. 4(a). However, inside the domain array, the domain width increases linearly with increasing pulse energy between 250 nJ and 500 nJ [Fig. 4(a)]. A similar dependence is observed when the length of the filaments is changed, while the pulse energy is kept at its maximum value of 550 nJ [cf. right column in Figs. 3(a) and 4(b)]. From the calibration data in Fig. 4, we have identified a pulse energy of 400 nJ and a depth of 100 μm to produce a 8×8 square domain grating with a lattice period of 20 μm. With these parameters, we expect small domains with a width of about 1–2 μm after thermal treatment. After selective chemical etching, the microscopy image of the lower surface of the crystal clearly reveals that all 64 domains are inverted and reach the bottom of the crystal [Fig. 5(a) (Multimedia view)]. This is also supported by the Čerenkov SHG microscopy image in Fig. 5(b). Again, we observe that the domains at the corners and at the borders are slightly broader than those in the middle of the grating. The complete domain structure is shown in 3D in Fig. 5(c) with the filaments on top of the domains.

We have seen that domains form below the filament when the laser focus is moved to the surface of the crystal. However, when the laser-induced filaments are located in the volume of the crystal, domains are inverted below and on top of the filaments as seen in Fig. 6. Here, the filaments have been induced with a pulse energy of 400 nJ in an addressed depth from 100 μm to 50 μm. Thus, the filaments are about 120 μm long and are located in the volume of the crystal. At the top [Fig. 6(a)] and at the bottom [Fig. 6(d)], one can see the formation of domains with their characteristic hexagonal shape after the thermal treatment. The same planes that are shown in Figs. 6(a) and 6(d) are imaged with the Čerenkov SHG microscope presented in Figs. 6(b) and 6(e). Figure 6(c) shows the plane of the induced filaments. The three slices along z are also marked in the 3D plot in Fig. 6(f). To investigate the resolution of this technique, we induced filaments close together with a pulse energy of 400 nJ at a depth of 100 μm. Figure 7 shows two microscopy images at the bottom of the crystal after selective chemical etching. When the distance of the filaments is around 2 μm, individual domains can still be separated below the filaments, although at the border, the domains merge [Fig. 7(a)]. Using a reduced filament spacing of 1 μm results in line domains [Fig. 7(b)]. We demonstrate the creation of arbitrary 2D domain patterns in the crystal volume by three examples shown in Fig. 8. Filaments were induced with laser pulses with an energy of 400 nJ at a depth of 80 μm. Note that all inverted domain structures are intact after several thermal treatments.

The results prove that ferroelectric domains are created in the whole volume of MgO-doped $\mathrm{LiNbO_3}$ crystals after thermal treatment without any external applied electric field. To explain this effect, we propose a model that is based on a pyroelectric field-assisted switching of the domains. It is known that a temperature change can cause domain back switching and domain wall motion in $\mathrm{LiNbO_3}$ and $\mathrm{LiTaO_3}$.[34–36] The net pyroelectric field E_{pyr} inside the crystal is the sum of the depolarizing field E_{dep} caused by the spontaneous polarization P_{s} and a screening field E_{scr}

$$E_{\mathrm{pyr}} = E_{\mathrm{dep}} + E_{\mathrm{scr}}\,.$$

At room temperature, the pyroelectric field is zero ($E_{\mathrm{net}} = 0$) because the depolarizing field is fully screened by bulk and surface charges [Fig. 9(a)]. While heating the crystal [Fig. 9(b)], the polarization decreases, and thus, the depolarizing field decreases as well, leading to a pyroelectric field in the direction of spontaneous polarization ($E_{\mathrm{net}} > 0$) with

$$E_{\mathrm{pyr}} = -\frac{1}{\epsilon\epsilon_0}\frac{\partial P_S}{\partial T}\Delta T.$$

Here, ΔT is the change in temperature. The dielectric constant of $\mathrm{LiNbO_3}$ is $\epsilon = 28$, and the pyroelectric coefficient

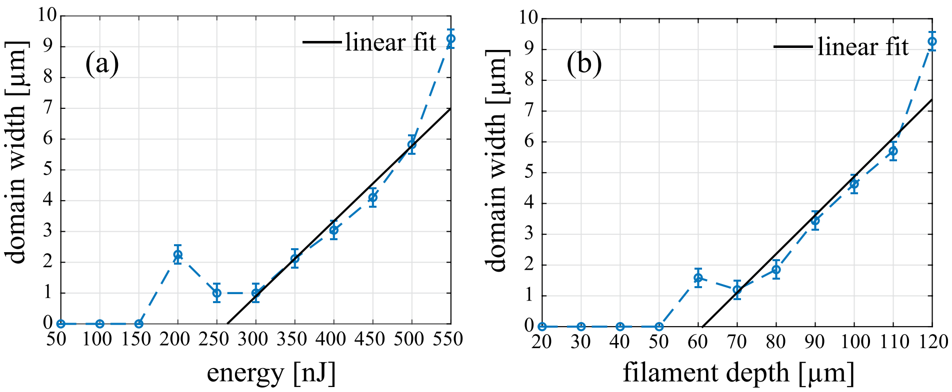

FIG. 4. Measured domain width. (a) Domain width as a function of pulse energy determined from the first row in Fig. 3(a). (b) Domain width as a function of addressed filament depth determined from the right column in Fig. 3(a). The lines are linear fits to the five measured values in this regime.

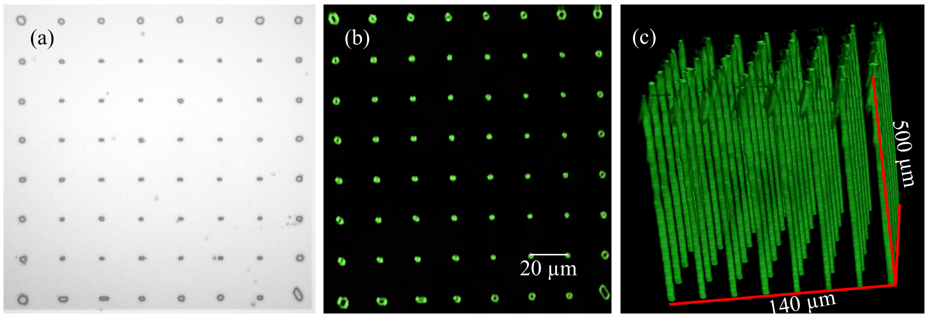

FIG. 5. Square lattice with a period of 20 μm. (a) Microscopy image of the lower surface of the crystal after selective chemical etching. (b) Čerenkov SHG microscopy image of the same plane as in (a). (c) The structure in the volume of the crystal measured in 3D with the Čerenkov SHG microscope. Multimedia view: https://doi.org/10.1063/1.5053870.1

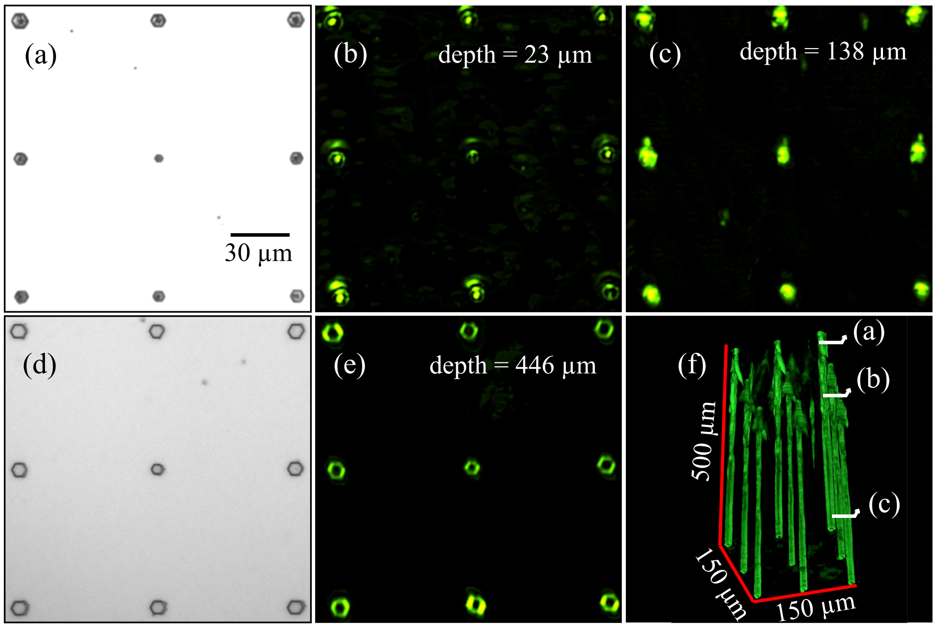

FIG. 6. Square lattice with a period of 50 μm. Microscopy image of the upper surface (a) and of the lower surface (d) after selective chemical etching. (b), (c), and (e) Čerenkov SHG microscopy images in three different depths. (f) The structure in the volume of the crystal measured in 3D with the Čerenkov SHG microscope. Multimedia view: https://doi.org/10.1063/1.5053870.2

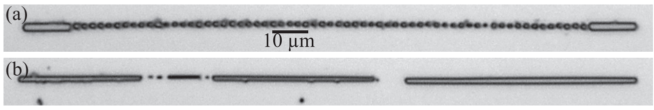

FIG. 7. Microscopy image of two domain lines at the bottom of the crystal after selective chemical etching. The distance between the laser-induced spots is 2 μm in (a) and 1 μm in (b).

$\partial P_S/\partial T = -0.83 \times 10^{-4}$ C/(m^2 K).[37] During heating, charges will be thermally activated that will drift into the net field, leading to a space charge field E_{sc-fil} in the vicinity of the filaments, thus compensating E_{net}. We assume a higher charge concentration inside the fs laser-induced filaments compared to the unmodified crystal volume. This charge concentration is higher for higher pulse energies and longer filaments, finally leading to a larger space charge field E_{sc-fil} and therefore to larger domains. The type of charges may be small polarons or ions such as protons or Li-ions. For instance, small polarons can occur in LiNbO$_3$[38] after thermal reduction. It has been proposed that a similar behavior occurs in fs laser-induced filaments.[31] However, to identify the nature of the charges, additional experiments such as Raman spectroscopy[39] are required which are beyond the scope of this paper. During the cooling process, spontaneous polarization increases again and E_{dep} immediately decays with the cooling rate [Fig. 9(c)]. The net field is now opposite to the spontaneous polarization. Domain formation occurs at a certain temperature, when E_{net} becomes larger than the threshold field of domain nucleation E_{thr}. For example, a temperature change of $\Delta T = 180\,^{\circ}$C will result in a pyroelectric field as high as 60 kV/mm. Thus, even if the pyroelectric field is partly compensated in the vicinity of the

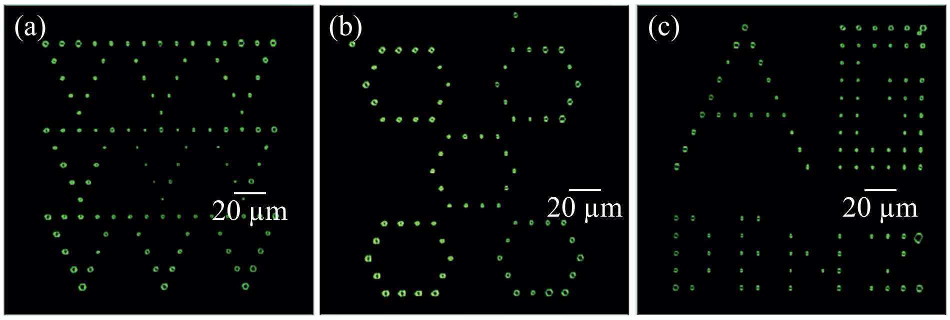

FIG. 8. Čerenkov SHG microscopy image of arbitrary 2D domain patterns at the bottom of the crystal after thermal treatment. (a) Triangles, (b) hexagons, and (c) letters.

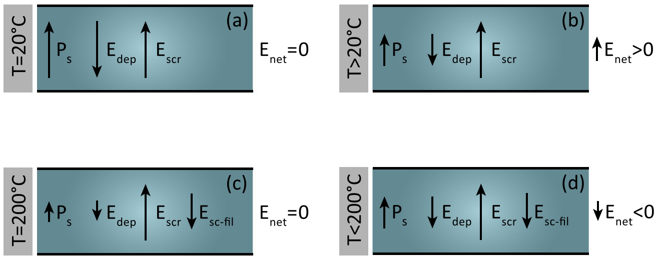

FIG. 9. Electric fields at room temperature (a), during heating (b), at 200 °C (c), and during cooling down (d) in the vicinity of the laser-induced filaments. During heating (b), a pyroelectric-field builds up ($E_{\text{net}} > 0$) and thermally activated charges drift in this net field and compensate it at 200 °C ($E_{\text{net}} = 0$) (c). During cooling down, E_{dep} decreases and the net field is now opposite to the spontaneous polarization and domain formation occurs when $E_{\text{net}} > E_{\text{thr}}$.

filaments, the net space charge field $E_{\text{sc-fil}}$ can become larger during cooling than the threshold field of domain nucleation. For comparison, the coercive field of MgO-doped $LiNbO_3$ decreases with increasing temperature and is about 4–5 kV/mm at room temperature.[40]

In conclusion, our approach proves that it is possible to invert long ferroelectric domains in the volume of MgO-doped $LiNbO_3$ crystals without any external applied electric field, solely by combining laser-induced filaments with a subsequent thermal treatment. The width of the domains can be controlled by the pulse energy and the length of the filaments. The domains can have a high aspect ratio of length/width of up to 800 μm/1 μm with all domain boundaries being straight over the entire domain length. The smallest achieved domain spacing is 1 μm, and lines of domains can also be inverted to produce 1D nonlinear photonic structures. We have proposed a model that is based on a pyroelectric field-assisted switching of the domains above and below permanent laser-induced defects. We are currently investigating the influence of temperature on the domain formation process in detail. Our approach has the potential to directly print arbitrary 2D ferroelectric domain structures by integrating fs-laser lithography and thermal treatment into a single setup. The principle of ferroelectric domain engineering by pyroelectric field-assisted fs-laser lithography is not limited to MgO-doped $LiNbO_3$. It can also be applied to other ferroelectric materials such as near-stoichiometric $LiTaO_3$ by adapting the experimental parameters.

[1] M. M. Fejer, G. A. Magel, D. H. Jundt, and R. L. Byer, IEEE J. Quantum Electron. **28**, 2631 (1992).

[2] N. G. R. Broderick, G. W. Ross, H. L. Offerhaus, D. J. Richardson, and D. C. Hanna, Phys. Rev. Lett. **84**, 4345 (2000).

[3] A. Arie and N. Voloch, Laser Photonics Rev. **4**, 355 (2010).

[4] S. Matsumoto, E. Lim, H. Hertz, and M. Fejer, Electron. Lett. **27**, 2040 (1991).

[5] M. Houe and P. D. Townsend, J. Phys. D: Appl. Phys. **28**, 1747 (1995).

[6] J. Thomas, V. Hilbert, R. Geiss, T. Pertsch, A. Tünnermann, and S. Nolte, Laser Photonics Rev. **7**, L17 (2013).

[7] S. Kroesen, K. Tekce, J. Imbrock, and C. Denz, Appl. Phys. Lett. **107**, 101109 (2015).

[8] D. Wei, C. Wang, H. Wang, X. Hu, D. Wei, X. Fang, Y. Zhang, D. Wu, Y. Hu, J. Li, S. Zhu, and M. Xiao, Nat. Photonics **12**, 596–600 (2018).

[9] C. Ying, A. Muir, C. Valdivia, H. Steigerwald, C. Sones, R. Eason, E. Soergel, and S. Mailis, Laser Photonics Rev. **6**, 526 (2012).

[10] A. Boes, D. Yudistira, T. Crasto, H. Steigerwald, V. Sivan, T. Limboeck, J. Friend, S. Mailis, E. Soergel, and A. Mitchell, Opt. Mater. Express **4**, 241 (2014).

[11] S. Zheng, Y. Kong, H. Liu, S. Chen, L. Zhang, S. Liu, and J. Xu, Opt. Express **20**, 29131 (2012).

[12] M. Fujimura, T. Sohmura, and T. Suhara, Electron. Lett. **39**, 719 (2003).

[13] C. L. Sones, M. C. Wengler, C. E. Valdivia, S. Mailis, R. W. Eason, and K. Buse, Appl. Phys. Lett. **86**, 212901 (2005).

[14] S. Mailis, P. Brown, C. Sones, I. Zergioti, and R. Eason, Appl. Phys. A: Mater. Sci. Process. **74**, 135 (2002).

[15] V. Y. Shur, Ferroelectrics **340**, 3 (2006).

[16] V. Y. Shur, D. K. Kuznetsov, A. I. Lobov, E. V. Nikolaeva, M. A. Dolbilov, A. N. Orlov, and V. V. Osipov, Ferroelectrics **341**, 85 (2006).

[17] A. C. Muir, C. L. Sones, S. Mailis, R. W. Eason, T. Jungk, A. Hoffman, and E. Soergel, Opt. Express **16**, 2336 (2008).

[18] V. Y. Shur, D. K. Kuznetsov, E. A. Mingaliev, E. M. Yakunina, A. I. Lobov, and A. V. Ievlev, Appl. Phys. Lett. **99**, 082901 (2011).

[19] A. Boes, T. Crasto, H. Steigerwald, S. Wade, J. Frohnhaus, E. Soergel, and A. Mitchell, Appl. Phys. Lett. **103**, 142904 (2013).

[20] D. Yudistira, A. Boes, A. R. Rezk, L. Y. Yeo, J. R. Friend, and A. Mitchell, Adv. Mater. Interfaces **1**, 1400006 (2014).

[21] X. Chen, P. Karpinski, V. Shvedov, K. Koynov, B. Wang, J. Trull, C. Cojocaru, W. Krolikowski, and Y. Sheng, Appl. Phys. Lett. **107**, 141102 (2015).

[22] X. Chen, P. Karpinski, V. Shvedov, A. Boes, A. Mitchell, W. Krolikowski, and Y. Sheng, Opt. Lett. **41**, 2410 (2016).

[23] T. Xu, K. Switkowski, X. Chen, S. Liu, K. Koynov, H. Yu, H. Zhang, J. Wang, Y. Sheng, and W. Krolikowski, Nat. Photonics **12**, 591–595 (2018).

[24] G. Zhou, A. Jesacher, M. Booth, T. Wilson, A. Ródenas, D. Jaque, and M. Gu, Opt. Express **17**, 17970 (2009).

[25] P. Karpinski, V. Shvedov, W. Krolikowski, and C. Hnatovsky, Opt. Express **24**, 7456 (2016).

[26] S. Kroesen, W. Horn, J. Imbrock, and C. Denz, Opt. Express **22**, 23339 (2014).

[27] R. R. Thomson, S. Campbell, I. J. Blewett, A. K. Kar, and D. T. Reid, Appl. Phys. Lett. **88**, 111109 (2006).

[28] J. Burghoff, H. Hartung, S. Nolte, and A. Tünnermann, Appl. Phys. A **86**, 165 (2006).

[29] J. Burghoff, S. Nolte, and A. Tünnermann, Appl. Phys. A **89**, 127 (2007).

[30] W. Yang, P. G. Kazansky, and Y. P. Svirko, Nat. Photonics **2**, 99 (2008).

[31] D. Paipulas, V. Kudriašov, M. Malinauskas, V. Smilgevičius, and V. Sirutkaitis, Appl. Phys. A **104**, 769 (2011).

[32] Y. Sheng, A. Best, H.-J. Butt, W. Krolikowski, A. Arie, and K. Koynov, Opt. Express **18**, 16539 (2010).

[33] M. Ayoub, H. Futterlieb, J. Imbrock, and C. Denz, Adv. Mater. **29**, 1603325 (2017).

[34] X. Liu, K. Kitamura, and K. Terabe, Appl. Phys. Lett. **89**, 142906 (2006).

[35] X. Y. Liu, K. Kitamura, Y. M. Liu, F. S. Ohuchi, and J. Y. Li, J. Appl. Phys. **110**, 052009 (2011).

[36] V. Y. Shur, E. A. Mingaliev, V. A. Lebedev, D. K. Kuznetsov, and D. V. Fursov, J. Appl. Phys. **113**, 187211 (2013).

[37] A. S. Bhalla and R. E. Newnham, Phys. Status Solidi **58**, K19 (1980).

[38] M. Imlau, H. Badorreck, and C. Merschjann, Appl. Phys. Rev. **2**, 040606 (2015).

[39] A. Ródenas, A. H. Nejadmalayeri, D. Jaque, and P. Herman, Opt. Express **16**, 13979 (2008).

[40] H. Ishizuki, I. Shoji, and T. Taira, Appl. Phys. Lett. **82**, 4062 (2003).